

Evidence of Fermi Surface Reconstruction at the Metamagnetic Transition of the Strongly Correlated Superconductor UTe_2

Q. Niu,¹ G. Knebel,¹ D. Braithwaite,¹ D. Aoki,^{1,2} G. Lapertot,¹ M. Vališka,¹
G. Seyfarth,³ W. Knafo,⁴ T. Helm,^{5,6} J-P. Brison,¹ J. Flouquet,¹ and A. Pourret^{1,*}

¹*Univ. Grenoble Alpes, CEA, IRIG, PHELIQS, F-38000 Grenoble, France*

²*Institute for Materials Research, Tohoku University, Oarai, Ibaraki, 311-1313, Japan*

³*Univ. Grenoble Alpes, EMFL, CNRS, Laboratoire National des
Champs Magnétiques Intenses (LNCMI), 38042 Grenoble, France*

⁴*Laboratoire National des Champs Magnétiques Intenses, UPR 3228,
CNRS-UPS-INSA-UGA, 143 Avenue de Rangueil, 31400 Toulouse, France*

⁵*Max Planck Institute for Chemical Physics of Solids, 01187 Dresden, Germany*

⁶*Dresden High Magnetic Field Laboratory (HLD-EMFL),
Helmholtz-Zentrum Dresden-Rossendorf, 01328 Dresden, Germany*

(Dated: March 23, 2020)

Thermoelectric power (S) and Hall effect (R_H) measurements on the paramagnetic superconductor UTe_2 with magnetic field applied along the hard magnetization b -axis are reported. The first order nature of the metamagnetic transition at $H_m = H_{c2}^b = 35$ T leads to drastic consequences on S and R_H . In contrast to the field dependence of the specific heat in the normal state through H_m , $S(H)$ is not symmetric with respect to H_m . This implies a strong interplay between ferromagnetic (FM) fluctuations and a Fermi-surface reconstruction at H_m . R_H is very well described by incoherent skew scattering above the coherence temperature T_m corresponding roughly to the temperature of the maximum in the susceptibility $T_{\chi_{\max}}$ and coherent skew scattering at lower temperatures. The discontinuous field dependence of both, $S(H)$ and the ordinary Hall coefficient R_0 , at H_m and at low temperature, provides evidence of a change in the band structure at the Fermi level.

PACS numbers: 71.18.+y, 71.27.+a, 72.15.Jf, 74.70.Tx

The recent discovery of unconventional superconductivity (SC) in the uranium chalcogenide paramagnet UTe_2 with a superconducting transition temperature $T_{\text{SC}} \sim 1.6$ K [1–3] opens new perspectives on superconducting topological properties including emergent Majorana quasiparticles at the verge of magnetic and electronic instability. Transport and thermodynamic measurements demonstrated that correlations play an important role in this system requiring theoretical treatment beyond LDA approach [2, 4–8]. The closeness of UTe_2 to a ferromagnetic quantum criticality [9] induces astonishing superconducting properties. Indeed when the magnetic field is applied along the hard b -axis at low temperature, superconductivity survives up to an extremely high field, $H_{c2} = 35$ T, where it is destroyed abruptly by the occurrence of a huge metamagnetic transition (MMT) at $H_m = H_{c2}$ [3, 10]. The unconventional superconducting state in this system, i.e. spin-triplet Cooper pairing, has been identified by a small decrease in the NMR Knight shift [11] and the large H_{c2} exceeding the Pauli-limiting field [1–3]. Furthermore, re-entrant superconductivity (RSC) arises above H_m when magnetic field is tilted 30° away from the b axis towards the c axis [10]. The MMT occurring at H_m with a jump in the magnetization of $0.6 \mu_B$, when the system enters the polarised paramagnetic state (PPM) [10, 12, 13], is in agreement with

a characteristic energy scale given by the temperature of the maximum in the susceptibility $T_{\chi_{\max}} \approx 35$ K [14] and the maximum of the Hall effect (R_H) [4]. Furthermore, fluctuations are strongly enhanced through H_m despite the first order nature of the MMT below the critical end point (CEP) at $T_{\text{CEP}} \approx 7$ K [12, 14].

By some aspects, UTe_2 has properties similar to that found in the unconventional ferromagnetic superconductor URhGe [15]. It shows similar field enhancement of the Sommerfeld coefficient γ (linear T term of the specific heat) associated to reentrant superconductivity (RSC) when approaching H_m ($H_m = H_T \approx 11.75$ T in URhGe) [16–18]. In URhGe, the MMT is connected to a Fermi-surface instability [19, 20] which may drive the SC [21, 22]. In UTe_2 as well as in URhGe, the MMT occurs for field along the hard magnetization axis. In both systems the MMT is strongly connected to the field enhancement of SC. A major difference is that URhGe is ferromagnetic with a Curie temperature $T_C = 9.5$ K at $H = 0$ while UTe_2 remains paramagnetic (PM) at least down to 20 mK [23, 24].

A key question is the respective roles of ferromagnetic fluctuations and Fermi-surface instabilities at the MMT where the SC is abruptly suppressed. Indeed, the large step-like increase of the residual term of the resistivity, ρ_0 , at the MMT suggests that in addition to magnetic fluctuations, a change in the carrier density may occur at the MMT for $H \parallel b$ [14]. For this purpose, we investigated the temperature and magnetic field dependences

* E-mail me at: alexandre.pourret@cea.fr

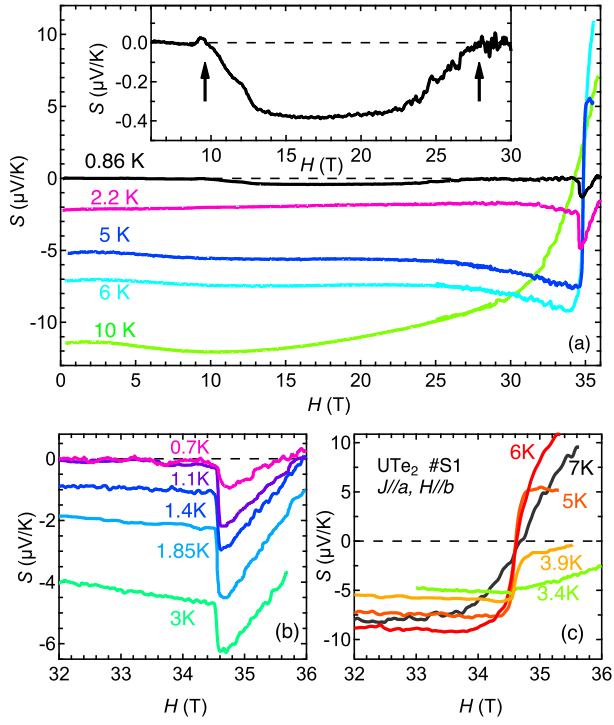


FIG. 1. (color online) Field dependence of S in UTe_2 for $H \parallel b$ between 0 and 36 T (a) and between 32 and 36 T (b-c). $S(H)$ shows a clear anomaly at $H_m = 34.6$ T, which broadens with increasing temperature. This anomaly changes from a negative to a positive jump above 3.5 K. The inset in (a) shows the RSC in $S(H)$ at 0.86 K in the field range from 6 T to 30 T.

of the Seebeck coefficient (S) up to 36 T and the Hall resistance (R_H) up to 68 T of UTe_2 for $H \parallel b$. RSC is observed in both S and R_H close to H_m around 1 K consistent with resistivity results [3]. The drastic changes in S and in the ordinary Hall effect (R_0) at H_m point to a Fermi-surface reconstruction, contrasting with the rather symmetric behaviour of the γ term [12] and of the A coefficient (T^2 term of the resistivity) through H_m [14].

Single crystals of UTe_2 were grown by chemical vapor transport with iodine as transport agent. The orientation of the crystals has been verified by Laue diffraction. We performed the S , ρ and R_H measurements on three samples labelled S1, S2 and S3 with a residual resistivity ratio ($\text{RRR} = \frac{\rho(300\text{ K})}{\rho(1.5\text{ K})}$) of 30, 30 and 22 respectively. The samples were prepared for experiments with heat or electric current along the a -axis and the magnetic field along the b -axis. S and R_H have been measured on sample S1 using a standard “one heater-two thermometers” setup and ρ_{xx} and R_H on sample S2 and S3 with a standard 6-probe method. The temperature and field dependences of different transport properties have been measured at LNCMI Grenoble using a ^3He cryostat up to 36 T and on sample S3 at LNCMI Toulouse in pulsed field up to

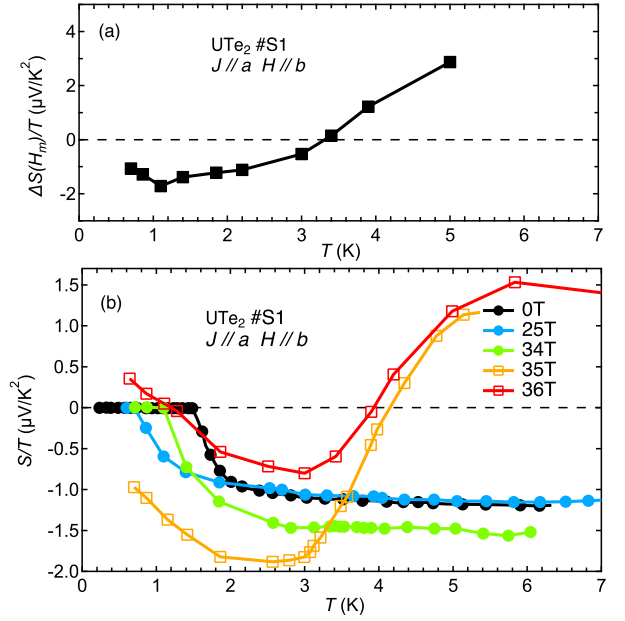


FIG. 2. (color online) (a) Magnitude of the jump $\Delta S/T = \frac{S(H_m + \delta H) - S(H_m - \delta H)}{T}$ in S/T at H_m . (b) Temperature dependence of S/T at different magnetic fields (full symbols $H < H_m$, open symbols $H > H_m$). S/T changes drastically with temperature near H_m .

68 T and temperature down to 1.5 K.

Figure 1 shows the magnetic field dependence of S from 0 to 36 T (a) and from 32 to 36 T (b-c) at various temperatures. At 0.7 K, S is equal to zero up to the first order transition at $H_m = 34.6$ T, where S shows a clear negative jump followed by a rapid increase in agreement with the collapse of SC above H_m . At slightly higher temperature 0.86 K, the sample enters the normal state at about 13 T with a negative S , as indicated by the arrows in the inset of Fig. 1 (a). A field-induced RSC phase is then observed between 27 T and 34.6 T. The first order character of the transition was also observed in our $S(H)$ measurements with a strong hysteresis, (see Fig. S1 of the Supplemental Material). Upon warming, the hysteresis closes and the jump vanishes, indicating that the first-order transition terminates at a CEP with $T_{\text{CEP}} \approx 7$ K in agreement previous measurements [12, 14]. Below T_{CEP} , there is a slight increase of $|S(H)|$ on approaching H_m , then $S(H)$ changes abruptly at H_m . Interestingly, the negative jump at H_m disappears at 3.4 K and it becomes positive at higher temperatures, as shown more clearly in Fig. 2 (a), where we plot $\Delta S(H_m)/T$ as a function of temperature up to 5 K. The amplitude of the transition increases up to $\approx 3\mu\text{V}/\text{K}^2$ at 5 K. For $T = 10$ K, above T_{CEP} only a large crossover can be detected.

Fig. 2 (b) shows the temperature dependence of $S(T)/T$ between 0 K and 7 K for different magnetic fields. For $H < H_m$ (full symbols), $S(T)/T \approx 1\mu\text{V}/\text{K}^2$

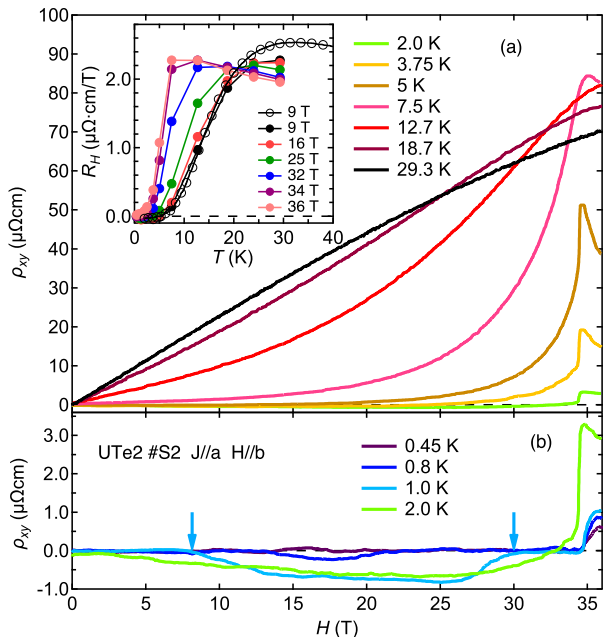


FIG. 3. (color online) (a) The Hall resistivity of UTe₂ with $H \parallel b$ up to 36 T at different temperatures. Panel (b) shows a zoom on low temperatures. The arrows indicate the normal state and RSC at 1 K. The inset of (a) shows the T dependence of the Hall coefficient at different field. Previous data are also represented (open circles) [4].

is temperature independent in the normal state in this temperature range and for field below 24 T. $|S(T)/T|$ is slightly larger on approaching H_m as shown for 34 T. In contrast, $S(T)/T$ displays a very different temperature dependence above H_m (open symbols). For instance, at 35 T, $S/T(T) < 0$ at low temperature (SC is suppressed) and decreases up to 3 K. Above 3 K, it increases drastically and changes sign at around 4.1 K. Moreover, at 36 T, the interesting feature is that S/T becomes positive at very low temperature below 1.4 K. This shows that at low temperature the sign of the dominant heat carriers changes through H_m from electrons to holes.

To extract more information about the field dependence of the carriers across H_m , we measured the Hall effect up to 36 T on sample S2 in static field and up to 68 T on sample S3 in pulsed field. Figure 3(a) and (b) show the H dependence of the Hall resistivity ρ_{xy} measured on S2 at different temperatures. At 0.45 K, the sample is superconducting up to the MMT. Above H_m , ρ_{xy} is positive in the normal state. At 1.0 K, RSC is detected in ρ_{xy} as indicated by the arrows. However, a negative ρ_{xy} shows up in the normal state below the RSC. As the temperature increases, the transition in ρ_{xy} at H_m becomes huge with a maximum value at 7.5 K near the CEP. At the same time, the initial slope of $\rho_{xy}(H)$ at low field also increases rapidly from negative to positive. The inset of Fig. 3 (a) illustrates the temperature de-

pendence of the Hall coefficient $R_H = \rho_{xy}/H$ at different fields. At 9 T, where $\rho_{xy}(H)$ is still linear, $R_H(T)$ changes rapidly from negative to positive and shows a maximum at $T_m \approx 30$ K close to $T_{\chi_{\max}}$ [4]. This drastic increase of the Hall coefficient at low temperature, which has been observed in many heavy fermion systems, like UPt₃ [25] and UAl₂ [26], is related to the change of the scattering process from incoherent skew scattering at high temperature to a coherent scattering regime at low temperature [27]. As H increases, $R_H(T)$ becomes steeper and T_m shifts to lower temperature until the MMT transition at H_m , where T_m ends at about 7 K close to the CEP (see also Fig. 5). Above H_m , R_H decreases with field and the temperature position of the maximum of R_H (labelled T_{cr}) is a signature of the PM-PPM crossover [19, 28]. It increases to higher temperature when increasing magnetic field (see Fig. S4 of the Supplemental Material).

In presence of magnetic fluctuations R_H can be described by the sum of an ordinary part R_0 and an anomalous part R_S . R_0 is simply related to the density and the mobility of the carriers while R_S is the result of different scattering processes. In heavy fermion systems, incoherent skew scattering of conduction electrons by independent local f moments predominates at high temperature above the coherence temperature [29]. R_S is proportional to the susceptibility χ and electrical resistivity ρ_{xx} , i.e. $R_S \propto \rho_{xx}\chi$. This has been verified in many materials in the high temperature incoherent regime. When the coherence settles in at low temperature, a different scattering mechanism, $R_S \propto \rho_{xx}^2\chi$ has been observed in many uranium heavy fermion compounds [26] and this is theoretically explained by coherent skew scattering [30].

In order to get information on the change of carriers in UTe₂ (for details see Supplemental Material), we have used susceptibility data of UTe₂ from Ref. 12 and plotted R_{xy}/H against $R_{xx}M/H$ or R_{xx}^2M/H at different temperatures (see Fig. S6, S7 and S8). R_{xy}/H is linear against R_{xx}^2M/H up to ~ 10 K. However, the curves below and above H_m fall onto two different lines with different slopes and/or intercepts, indicating that both R_0 and R_S have discontinuous changes at H_m . In contrast on, at 50 K, which is above T_m , the coherence temperature, R_{xy}/H is on a straight line with $R_{xx}M/H$ in almost the whole field range, consistent with the incoherent skew scattering predictions. The analysis shows that the Hall effect below 10 K is dominated by coherent and above 10 K by incoherent skew scattering. This allows us to estimate the contribution of R_0 to the total Hall effect. The solid lines in Fig. 4 (a) show R_{xy}/H , while the dashed lines correspond to the anomalous Hall contribution obtained from the fitting by considering the change of slope of the anomalous Hall effect below (short dash) and above (long dash) H_m . The difference of these two datasets gives an estimation of R_0 as plotted in Fig. 4 (b). At 1.4 K, below H_m , R_0 reflects the fact that the anomalous Hall effect vanishes at low temperature (see also Fig. S5).

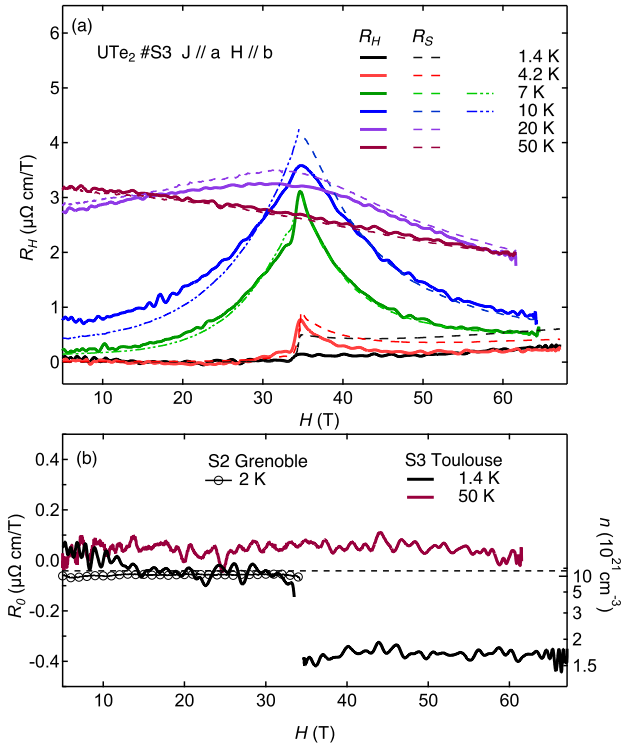


FIG. 4. (color online) (a) The Hall coefficient of UTe₂ S3 with $H \parallel b$ up to 68 T (pulsed field). The dashed lines are estimated from the coherent ($T < 20$ K) and incoherent ($T \geq 20$ K) skew scattering at different temperatures respectively. For $T < 20$ K, the long and short dashes correspond to the anomalous Hall signal obtained above and below H_m respectively. (b) R_0 is obtained after subtracting the anomalous part from the Hall signal (additional temperature are shown on Fig. S9). The right scale indicates the carrier density and the dashed line represents the value obtained previously [4].

R_0 is negative, very small, and independent of magnetic field up to H_m . The value of the extracted carrier density (right scale) is in good agreement with the value obtained previously (dashed line) [4], $n = 1.6 \times 10^{22} \text{ cm}^{-3}$. Above H_m , $|R_0|$ is much larger and still field independent. Most likely, such a behaviour is the signature of a change of the carrier density (accompanied or not with a change of the mobility) at the MMT. In contrast, at 50 K entering in the incoherent regime, the Hall coefficient can be very well reproduced by anomalous Hall terms.

$H_{c2}(T)$ and H_m detected in S and ρ are summarised in the H - T phase diagram in Fig. 5. $H_{c2}(T)$ is defined by $S = 0$ or $\rho = 0$. Above 10 T, S and ρ show an almost vertical $H_{c2}(T)$ between 10 T and 28 T and H_{c2} is strongly enhanced, reaching 1.4 K at H_m , consistent with previous resistivity experiments [1, 3]. The temperatures of the maximum of the Hall effect, T_m (similar to $T_{\chi_{\max}}$) and T_{cr} are also represented. This is similar to the energy scales observed near the tri-critical point in the ferromagnetic superconductor URhGe with the same

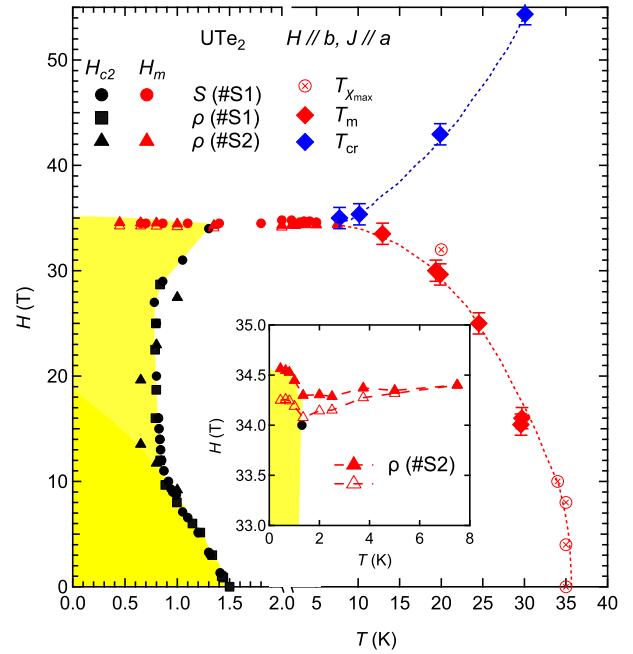


FIG. 5. (color online) H - T phase diagram of UTe₂ for $H \parallel b$. H_{c2} from different samples by black symbols and the metamagnetic field H_m was labelled by red circles (S) and red triangles (ρ). Red crosses, red diamonds and blue diamonds indicate $T_{\chi_{\max}}$, T_m and T_{cr} respectively. The inset shows a zoom very close to H_m . Full symbols are from increasing field sweeps, open symbols from downward field sweeps. SC survives slightly above the MMT.

crossover line separating PM and PPM states [19]. Similar TEP experiments in the nearly ferromagnetic (FM) case of UCoAl [31] have identified the CEP of the first order transition at the MMT from PM to FM states. This material is an itinerant Ising system, where the MMT occurs with H along the Ising axis. In contrast, in UTe₂ as well as in URhGe, the MMT occurs for field along the hard magnetization axis. In both systems the MMT is strongly connected to the field enhancement of SC. The inset magnifies the phase diagram near the MMT transition. We observe that H_m (H_{c2}) has an upturn below 1 K. This new feature indicates that SC persists above the extrapolation of H_m to $T = 0$ K, although in a very narrow field range.

In conclusion, we have studied the thermoelectric power and the Hall effect of PM superconductor UTe₂ up to 36 T and 68 T respectively, with magnetic field along hard magnetization b -axis. RSC was observed in both S and R_H at low temperature on approaching the MMT. R_H is very well described by incoherent skew scattering above the coherence temperature T_M which corresponds roughly to $T_{\chi_{\max}}$ and coherent skew scattering at lower temperature. The correspondence of these two energy scale highlights the dual character, localized-itinerant,

of the f electrons in uranium compounds. Below this Kondo coherence temperature, DFT calculations reveal the emergence of a band structure with a small peak in the density of states at the Fermi level [32]. The field dependence of R_H suggests the suppression of well defined coherent scattering by strong magnetic fluctuations near the MMT. Above T_{SC} , for $H < H_m$, the anomalous part of the Hall signal vanishes, opposite to the case $H > H_m$ where the anomalous part is still present. The strong change of R_0 and S evidence a Fermi-surface reconstruction at H_m . As this Fermi surface change leads to the vanishing of SC above H_m , a drastic change in the nature of the SC pairing may happen, contrasting with rather symmetrical variation of $\gamma(H)$ on crossing H_m . A still open question is the anomalous SC phase which persists at 30° from the b axis in the PPM states above H_m . The originality of UTe_2 consists in its proximity to a Kondo-lattice metal-insulator instability which deserves to be studied further under both magnetic field and pressure.

The authors thank K. Izawa, S. Hosoi, H. Harima, J. Ishizuka, Y. Yanase, for stimulating discussions. We acknowledge A. Miyake for high magnetic field magnetization data. This work has been supported by the Université Grenoble Alpes and KAKENHI (JP15H0082, JP15H0084, JP15K21732, JP19H00646, JP16H04006, JP15H05745). We acknowledge support of the LNCMI-CNRS, member the European Magnetic Field Laboratory (EMFL).

-
- [1] S. Ran, C. Eckberg, Q.-P. Ding, Y. Furukawa, T. Metz, S. R. Saha, I.-L. Liu, M. Zic, H. Kim, J. Paglione, and N. P. Butch, *Science* **365**, 684 (2019).
- [2] D. Aoki, A. Nakamura, F. Honda, D. Li, Y. Homma, Y. Shimizu, Y. J. Sato, G. Knebel, J.-P. Brison, A. Pourret, D. Braithwaite, G. Lapertot, Q. Niu, M. Vališka, H. Harima, and J. Flouquet, *J. Phys. Soc. Jpn.* **88**, 043702 (2019).
- [3] G. Knebel, W. Knafo, A. Pourret, Q. Niu, M. Vališka, D. Braithwaite, G. Lapertot, M. Nardone, A. Zitouni, S. Mishra, I. Sheikin, G. Seyfarth, J.-P. Brison, D. Aoki, and J. Flouquet, *J. Phys. Soc. Jpn.* **88**, 063707 (2019).
- [4] Q. Niu, G. Knebel, D. Braithwaite, D. Aoki, G. Lapertot, G. Seyfarth, J.-P. Brison, J. Flouquet, and A. Pourret, *Phys. Rev. Lett.* **124**, 086601 (2020).
- [5] J. Ishizuka, S. Sumita, A. Daido, and Y. Yanase, *Phys. Rev. Lett.* **123**, 217001 (2019).
- [6] S.-i. Fujimori, I. Kawasaki, Y. Takeda, H. Yamagami, A. Nakamura, Y. Homma, and D. Aoki, *J. Phys. Soc. Jpn.* **88**, 103701 (2019).
- [7] Y. Xu, Y. Sheng, and Y. F. Yang, *Phys. Rev. Lett.* **123**, 217002 (2019).
- [8] L. Miao, S. Liu, Y. Xu, E. C. Kotta, C.-J. Kang, S. Ran, J. Paglione, G. Kotliar, N. P. Butch, J. D. Denlinger, and L. A. Wray, *Phys. Rev. Lett.* **124**, 076401 (2020).
- [9] Y. Tokunaga, H. Sakai, S. Kambe, T. Hattori, N. Higa, G. Nakamine, S. Kitagawa, K. Ishida, A. Nakamura, Y. Shimizu, Y. Homma, D. Li, F. Honda, and D. Aoki, *J. Phys. Soc. Jpn.* **88**, 073701 (2019).
- [10] S. Ran, I.-L. Liu, Y. S. Eo, D. J. Campbell, P. M. Neves, W. T. Fuhrman, S. R. Saha, C. Eckberg, H. Kim, D. Graf, F. Balakirev, J. Singleton, J. Paglione, and N. P. Butch, *Nat. Phys.* **15**, 1250 (2019).
- [11] G. Nakamine, S. Kitagawa, K. Ishida, Y. Tokunaga, H. Sakai, S. Kambe, A. Nakamura, Y. Shimizu, Y. Homma, D. Li, F. Honda, and D. Aoki, *J. Phys. Soc. Jpn.* **88**, 113703 (2019).
- [12] A. Miyake, Y. Shimizu, Y. J. Sato, D. Li, A. Nakamura, Y. Homma, F. Honda, J. Flouquet, M. Tokunaga, and D. Aoki, *J. Phys. Soc. Jpn.* **88**, 063706 (2019).
- [13] S. Imajo, Y. Kohama, A. Miyake, C. Dong, M. Tokunaga, J. Flouquet, K. Kindo, and D. Aoki, *J. Phys. Soc. Jpn.* **88**, 083705 (2019).
- [14] W. Knafo, M. Vališka, D. Braithwaite, G. Lapertot, G. Knebel, A. Pourret, J.-P. Brison, J. Flouquet, and D. Aoki, *J. Phys. Soc. Jpn.* **88**, 063705 (2019).
- [15] D. Aoki, A. Huxley, E. Ressouche, D. Braithwaite, J. Flouquet, J. P. Brison, E. Lhotel, and C. Paulsen, *Nature* **413**, 613 (2001).
- [16] A. Miyake, D. Aoki, and J. Flouquet, *J. Phys. Soc. Jpn.* **77**, 094709 (2008).
- [17] F. Hardy, D. Aoki, C. Meingast, P. Schweiss, P. Burger, H. v. Löhneysen, and J. Flouquet, *Phys. Rev. B* **83**, 195107 (2011).
- [18] B. Wu, G. Bastien, M. Taupin, C. Paulsen, L. Howald, D. Aoki, and J.-P. Brison, *Nat. Commun.* **8**, 14480 (2017).
- [19] A. Gourgout, A. Pourret, G. Knebel, D. Aoki, G. Seyfarth, and J. Flouquet, *Phys. Rev. Lett.* **117**, 046401 (2016).
- [20] D. Aoki, G. Knebel, and J. Flouquet, *J. Phys. Soc. Jpn.* **83**, 094719 (2014).
- [21] E. a. Yelland, J. M. Barraclough, W. Wang, K. V. Kamenev, and a. D. Huxley, *Nat. Phys.* **7**, 890 (2011).
- [22] Y. Sherkunov, A. V. Chubukov, and J. J. Betouras, *Phys. Rev. Lett.* **121**, 097001 (2018).
- [23] S. Sundar, S. Gheidi, K. Akintola, A. M. Côté, S. R. Dunsiger, S. Ran, N. P. Butch, S. R. Saha, J. Paglione, and J. E. Sonier, *Phys. Rev. B* **100**, 140502 (2019).
- [24] C. Paulsen, G. Knebel, G. Lapertot, D. Braithwaite, A. Pourret, D. Aoki, F. Hardy, J. Flouquet, and J. P. Brison, *arXiv:2002.12724* (2020).
- [25] J. Schoenes and J. J. M. Franse, *Phys. Rev. B* **33**, 5138 (1986).
- [26] M. HadžićLeroux, A. Hamzić, A. Fert, P. Haen, F. Lapierre, and O. Laborde, *Europhys. Lett.* **1**, 579 (1986).
- [27] Y.-F. Yang, *Phys. Rev. B* **87**, 45102 (2013).
- [28] A. Palacio Morales, A. Pourret, G. Seyfarth, M.-T. Suzuki, D. Braithwaite, G. Knebel, D. Aoki, and J. Flouquet, *Physical Review B* **91**, 245129 (2015).
- [29] A. Fert and P. M. Levy, *Phys. Rev. B* **36**, 1907 (1987).
- [30] K. Yamada, K. Ani, H. Kohno, and S. Inagaki, *Prog. Theor. Phys.* **89** (1993).
- [31] A. Palacio-Morales, A. Pourret, G. Knebel, T. Combier, D. Aoki, H. Harima, and J. Flouquet, *Phys. Rev. Lett.* **110**, 116404 (2013).
- [32] L. Miao, S. Liu, Y. Xu, E. C. Kotta, C.-J. Kang, S. Ran, J. Paglione, G. Kotliar, N. P. Butch, J. D. Denlinger, and L. A. Wray, *Phys. Rev. Lett.* **124**, 076401 (2020).

Supplemental Material: Evidence of Fermi Surface Reconstruction at the Metamagnetic Transition of the Strongly Correlated Superconductor UTe_2

Q. Niu,¹ G. Knebel,¹ D. Braithwaite,¹ D. Aoki,^{1,2} G. Lapertot,¹ M. Vališka,¹
G. Seyfarth,³ W. Knafo,⁴ T. Helm,^{5,6} J-P. Brison,¹ J. Flouquet,¹ and A. Pourret¹

¹Univ. Grenoble Alpes, CEA, IRIG, PHELIQS, F-38000 Grenoble, France

²Institute for Materials Research, Tohoku University, Oarai, Ibaraki, 311-1313, Japan

³Univ. Grenoble Alpes, EMFL, CNRS, Laboratoire National des Champs Magnétiques Intenses (LNCMI), 38042 Grenoble, France

⁴Laboratoire National des Champs Magnétiques Intenses, UPR 3228, CNRS-UPS-INSA-UGA, 143 Avenue de Rangueil, 31400 Toulouse, France

⁵Max Planck Institute for Chemical Physics of Solids, 01187 Dresden, Germany

⁶Dresden High Magnetic Field Laboratory (HLD-EMFL),

Helmholtz-Zentrum Dresden-Rossendorf, 01328 Dresden, Germany

(Dated: March 23, 2020)

I. Hysteresis in $S(H)$ of UTe_2 at H_m

With the same configuration as described in the main text, we measured $S(H)$ in a narrow field range near H_m sweeping the field up and down through H_m with lower ramping rate. Fig. S1 shows the results at different temperatures up to 10 K. A hysteresis is clearly observed at low temperatures revealing the first-order character of the metamagnetic transition (MMT). The vanishing of the hysteresis with increasing temperature indicates that the first-order transition terminates at the critical end point (CEP) with $T_{\text{CEP}} \approx 7$ K.

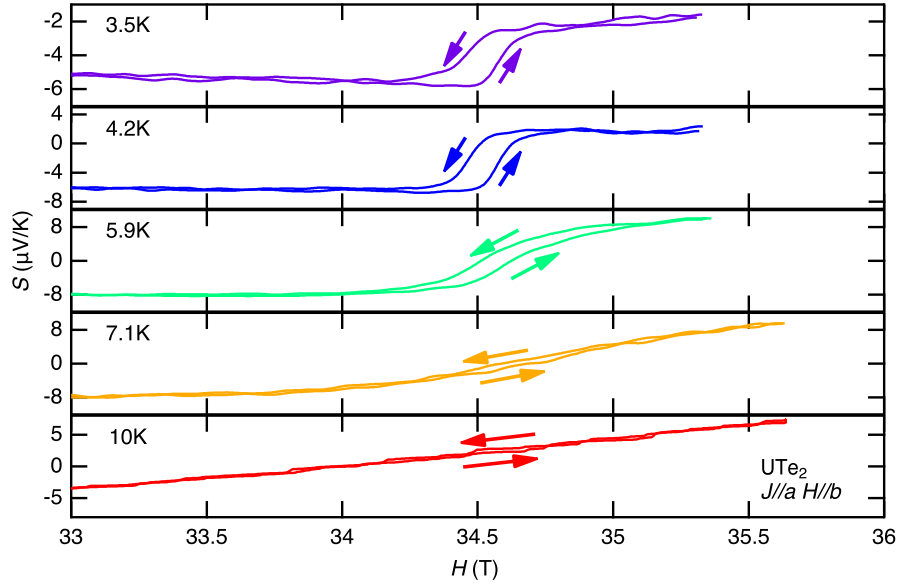


FIG. S1: (color online) Temperature evolution of the hysteresis observed in S at H_m . The arrows indicate the direction of the field sweep. The first-order transition ends at the critical end point $T_{\text{CEP}} \approx 7$ K.

II. Resistivity and Hall signal for $H \parallel b$

Resistivity and Hall effect have been measured on sample S2 and S3, part of the results have been already shown in the main text. Fig. S2(a) shows the magnetic field dependence of R_{xx} for different temperatures up to 36 T for sample S2. Below 1.5 K, R_{xx} is zero up to H_m and then shows a step like anomaly indicating that $H_{\text{C}2}$ is equal to H_m for $H \parallel b$. By increasing temperature, R_{xx} is non zero below H_m but still shows a step like anomaly at the MMT up to $T_{\text{CEP}} \approx 7$ K. Above T_{CEP} , the transition broadens significantly. The first order character of the transition below

T_{CEP} is also confirmed by the observation of an hysteresis loop in the resistivity, see Fig. S2(b). Interestingly, as soon as the system becomes superconducting below 1.5 K, the width of the transition broadens and the superconducting transition seems to move to higher field, conserving a hysteresis loop. The field dependence of R_{xx} and R_{xy} up to 68 T of sample S3 are represented in Fig. S3. The resistivity data are similar to sample S2. At low temperature, R_{xy} is almost field independent below H_m , shows a small step like anomaly at H_m and becomes field dependent above H_m . By increasing temperature, the transition becomes a peak which is very sharp at $T_{\text{CEP}} \approx 7$ K and broadens for high temperature. Fig. S4 shows the temperature dependence of the Hall coefficient R_H measured on sample S3. From low magnetic field, the temperature of the maximum in $R_H(T)$, defined as T_m shifts to low temperature when approaching H_m down to T_{CEP} . Above H_m , the temperature of the maximum T_{cr} , corresponding to the crossover temperature between the PM and PPM state, shifts to higher temperature. The energy scale associated to T_m (similar to $T_{\chi_{\text{max}}}$) doesn't decrease to zero temperature but is limited to T_{CEP} due to the first order nature of the transition and so to the absence of a quantum critical point.

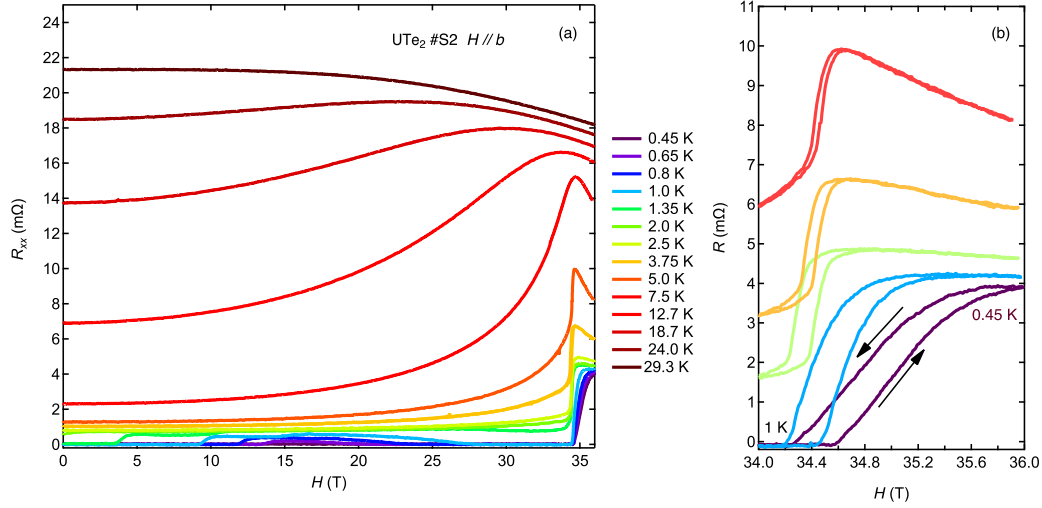


FIG. S2: (color online) (a) Field dependence of R_{xx} on sample S2 up to 36 T at different temperatures for $H \parallel b$. (b) Hysteresis loop of R_{xx} at the metamagnetic transition highlighting the first order character of the transition below $T_{\text{CEP}} \approx 7$ K.

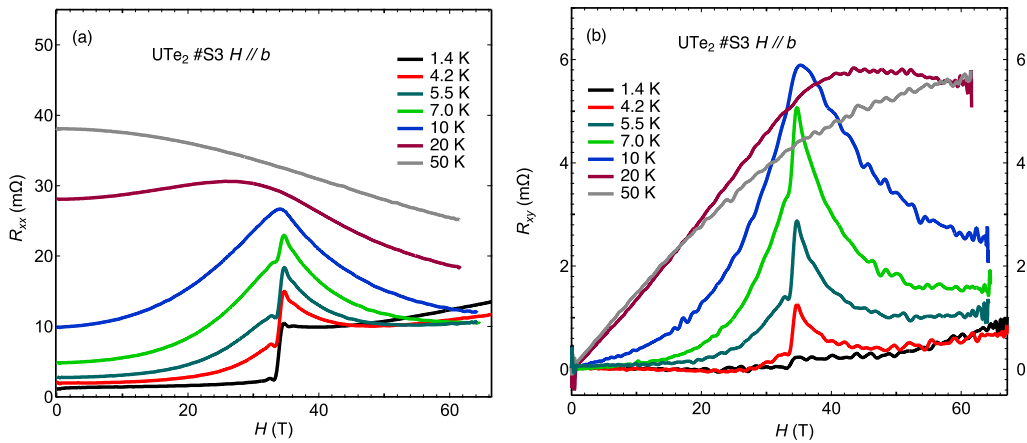


FIG. S3: (color online) Field dependence of R_{xx} (a) and R_{xy} (b) on sample S3 up to 68 T at different temperatures.

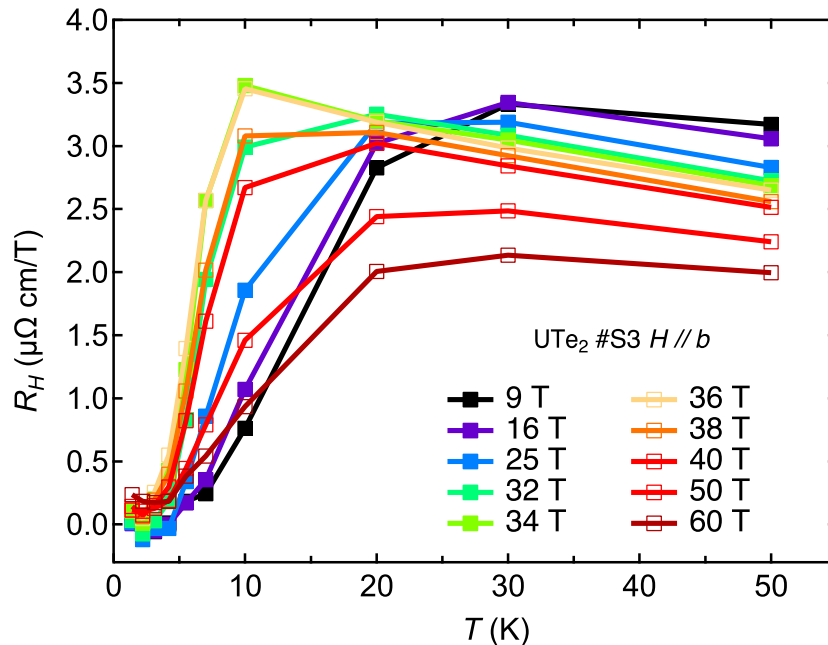


FIG. S4: (color online) Temperature dependence of R_H on sample S3 at different magnetic fields for $H < H_m$ (full symbols) and for $H > H_m$ (open symbols).

III. Ordinary and anomalous Hall effect

Here we describe the procedure to estimate the ordinary and anomalous contribution to the Hall effect. The first assumption is that the Hall signal is the sum of two terms, $R_H = R_0 + R_S$ where R_0 is the ordinary part associated to de density of carriers and their mobility and R_S is the anomalous part associated to scattering processes on magnetic impurities. The microscopic origin of R_S is quite complex. Three distinct contributions, intrinsic, skew scattering, and side jump scattering have been identified. Each of them has an individual scaling $R_S \propto \rho^\alpha M_z/H$ with respect to the longitudinal resistivity ρ . Here, M_z is the magnetization and H the magnetic field along z axis. In ferromagnetic materials, the summation of the three terms yields an empirical formula that explains a large amount of experimental data. However, in heavy fermion materials a satisfactory formula has not been achieved nevertheless it have been observed that the skew scattering is the dominant scattering process with two different scaling depending of the temperature^{S1,S2}. At high temperature, for $T > T^*$ (coherence temperature), the incoherent skew scattering of conduction electrons by independent f electrons should be considered and then the relation $R_S = C' \times \rho M/H$ is expected. On the other hand, at low temperature for $T < T_{FL}$ (Fermi liquid temperature) a different scaling is expected, $R_S = C \times \rho^2 M/H$, due to the coherent skew scattering of f electrons once the Fermi surface is well defined. Between T^* and T_{FL} a cross-over regime is observed. In Fig. S5, the temperature dependence of R_H is represented. The inset shows that as expected at low temperature (for $T < 20$ K), the Hall signal is well described by a linear fitting as a function of $\rho^2 M/H$ indicating that below $T_{\chi_{max}}$, a coherent regime appears. The fact that the fit (R_S_LT) is smaller than the R_H data at very low temperatures indicates that the anomalous contribution to the Hall signal is negligible at low temperature, and justifies to extract the number of carriers by using the Hall signal above T_{SC} in this material^{S3}. The fit using $\rho M/H$, (R_S_HT), is not very satisfactory at high temperature. This discrepancy can be explained by the phonon contribution in the resistivity^{S1}.

To extract the coefficients C and C' , we have plotted R_{xy}/H as a function of $R_{xx}M/H$ in figure Fig. S6 and as a function of R_{xx}^2M/H in Fig. S7. We observe that for $T < 20$ K, the data are well described by R_{xx}^2M/H meaning that below T^* (roughly $T_{\chi_{max}}$), the anomalous Hall signal is well described by coherent skew scattering of f electrons. For high temperature, the anomalous Hall signal is well described by $R_{xx}M/H$ underlying the predominance of incoherent skew scattering processes above T^* . These observations are summarised in Fig. S8 where R_{xy}/H is plotted either as a function of $R_{xx}M/H$ or R_{xx}^2M/H depending on the temperature. It is interesting to notice that for $T > 20$ K, for the whole magnetic field range, the data are well fitted by an unique linear function of $R_{xx}M/H$ passing through the origin meaning that the ordinary Hall effect is negligible at high temperature. At low temperature, the data are clearly well described by two linear functions of R_{xx}^2M/H below and above H_m . The value of the coefficients C and

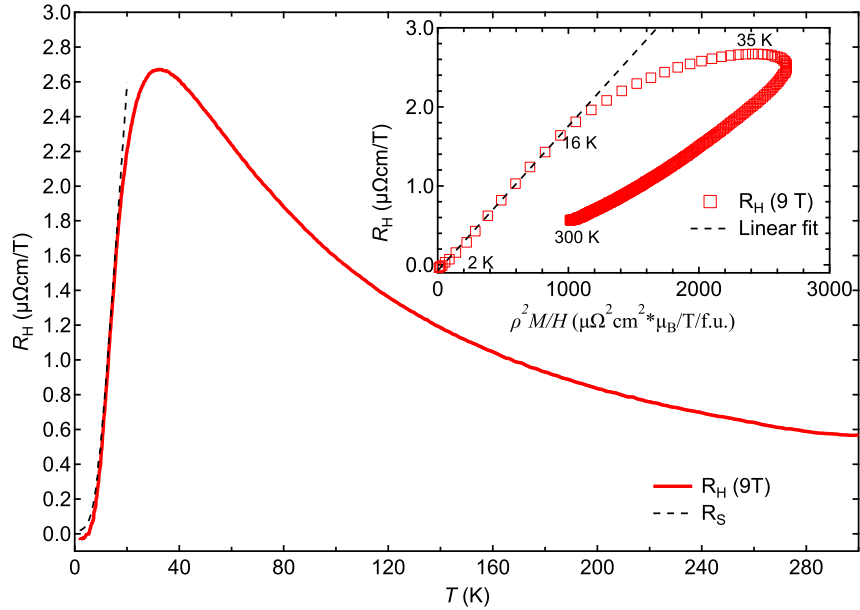


FIG. S5: (color online) Temperature dependence of R_H between 1.4 K and 300 K. The different fitting curves for the anomalous Hall effect at low temperature ($\propto \rho^2 M/H$) and high temperature ($\propto \rho M/H$) are represented (dashed lines). Inset: R_H as a function of $\rho^2 M/H$. The dash line represents linear fitting.

TABLE S1: List of anomalous Hall effect coefficients C ($R_S = C \times \rho^2 M/H$) for H below and above H_m and C' ($R_S = C' \times \rho M/H$).

T (K)	C (arb. units)		$C(H > H_m)/C(H < H_m)$
	$H < H_m$	$H > H_m$	
1.4	65.3	8.6	0.13
4.2	18.4	7.6	0.41
7	21.1	10.2	0.48
10	13.9	10.5	0.75
	C' (arb. units)		
20	0.30		
50	0.22		

C' are summarised in table S1. The variation of C indicates that the amplitude of the scattering changes through H_m . At 1.4 K, below H_m the data don't show any linear dependence meaning that the Hall signal is ordinary. On the other hand, above H_m , the data show still linear dependence meaning that even at very low temperature, there is still a contribution from the anomalous Hall effect above the metamagnetic transition just above T_{SC} .

After extracting the contribution of the anomalous Hall effect, through the different coefficients C and C' depending on the temperature, we obtained the ordinary contribution by subtracting the anomalous part from the raw data by taking into account the change of the coefficient C through H_m . For all temperatures, the field dependence of the ordinary Hall effect is represented in Fig. S9. A drastic change of the ordinary Hall effect at H_m is extracted from this analysis indicating a change of the number of carriers associated or not with a change of their mobility.

[S1] A. Fert and P. M. Levy, Phys. Rev. B **36**, 1907 (1987).

[S2] Y.-F. Yang, Phys. Rev. B **87**, 45102 (2013).

[S3] Q. Niu, G. Knebel, D. Braithwaite, D. Aoki, G. Lapertot, G. Seyfarth, J.-P. Brison, J. Flouquet, and A. Pourret, Phys. Rev. Lett. **124**, 086601 (2020).

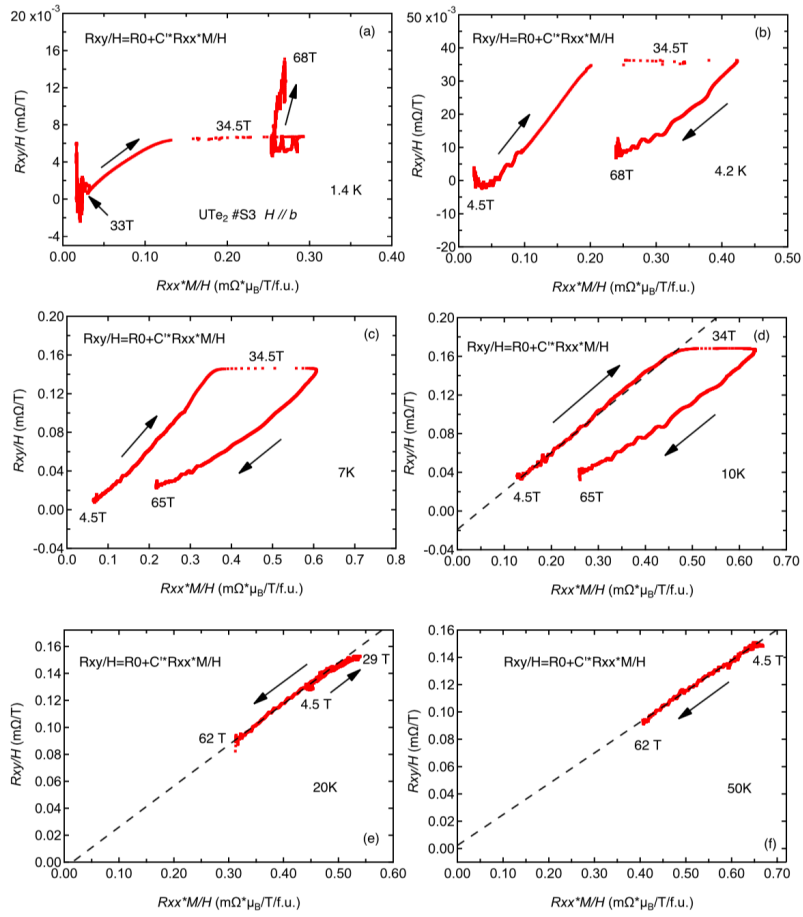


FIG. S6: (color online) R_{xy}/H against $R_{xx}M/H$. The dashed lines are linear fits.

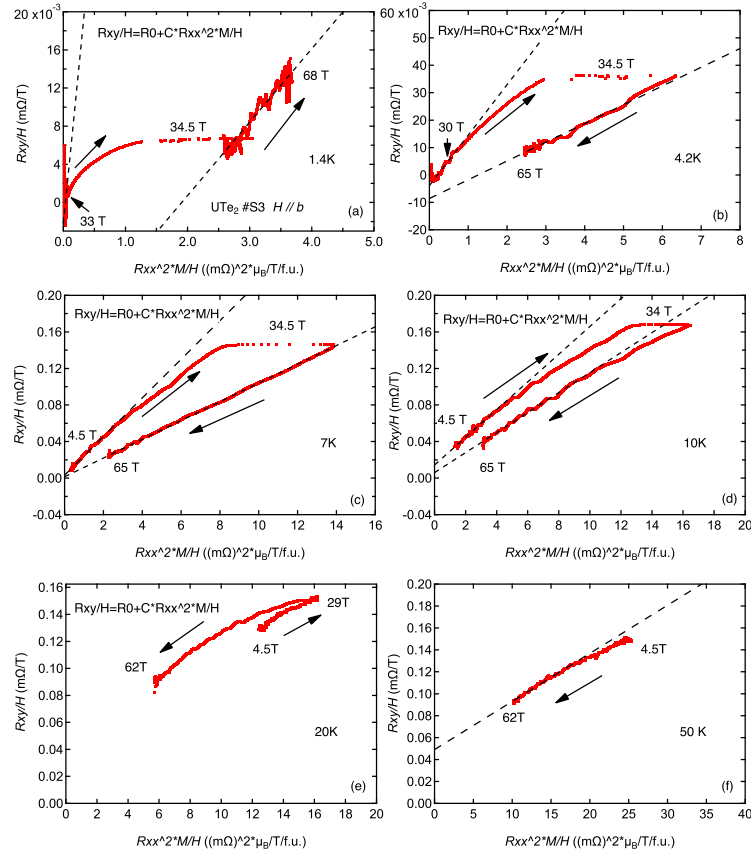


FIG. S7: (color online) R_{xy}/H against R_{xx}^2M/H . The dashed lines are linear fits.

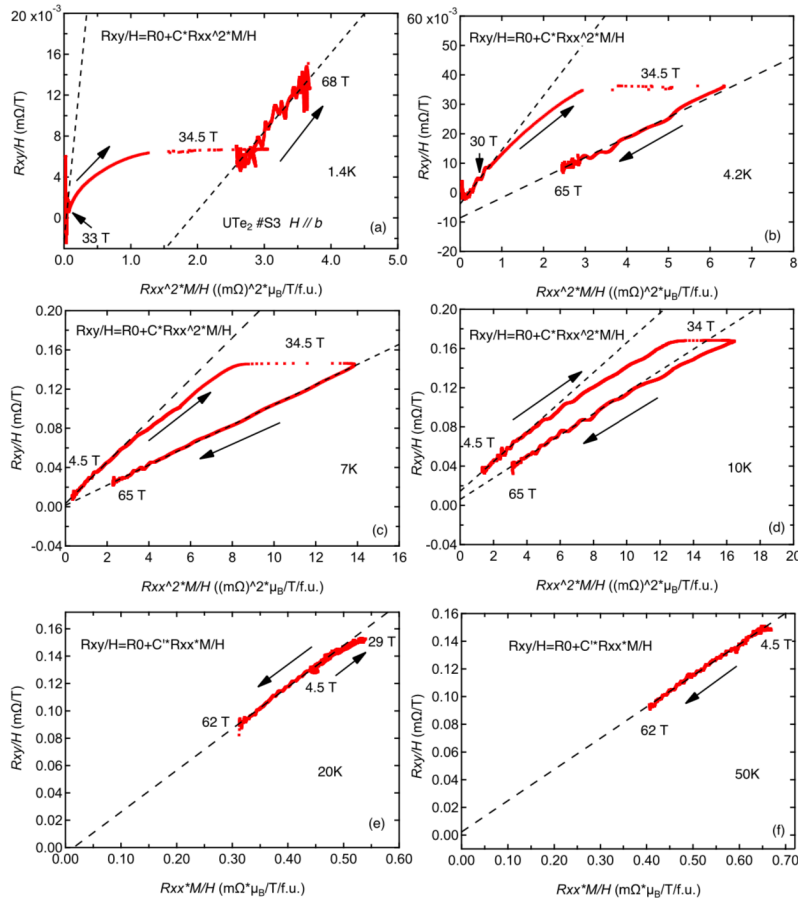


FIG. S8: (color online) R_{xy}/H against $R_{xx}^2 M/H$ at 1.4 K, 4.2 K, 7 K and 10 K. R_{xy}/H against $R_{xx} M/H$ at 20 K and 50 K. The dashed lines are linear fits.

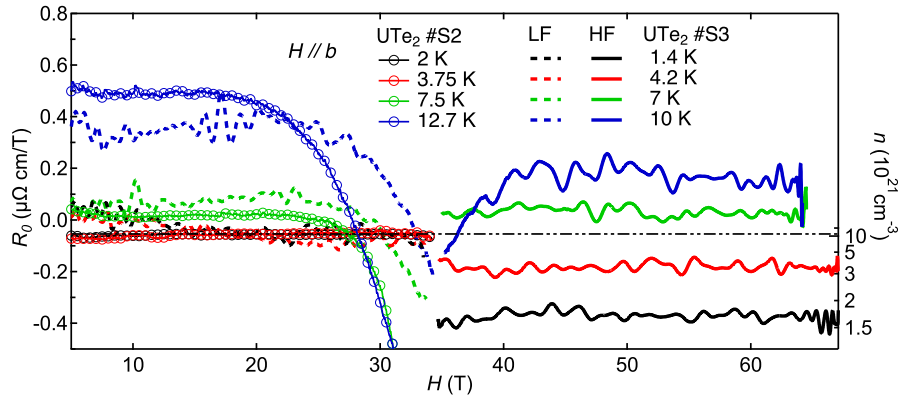


FIG. S9: (color online) Complement to Fig. 4 b) of main text. Ordinary Hall effect as a function of magnetic field for different temperatures obtained after subtracting the anomalous contribution (taking into account its change of amplitude through H_m). This implies two sets of data for low field (dashed lines LF) and high field (full lines HF) for the sample S3 measured up to 68 T. The right scale indicates the carrier density and the dashed-dot line represents the value obtained previously^{S3}.